NÖHÜ Müh. Bilim. Derg. / NOHU J. Eng. Sci., 2023; 12(3), 957-964

Niğde Ömer Halisdemir Üniversitesi Mühendislik Bilimleri Dergisi
Niğde Ömer Halisdemir University Journal of Engineering Sciences

Araştırma makalesi / Research article

www.dergipark.org.tr/tr/pub/ngumuh / www.dergipark.org.tr/en/pub/ngumuh

Effect of $SnCl_2$ heat treatment on SnS thin films deposited by RF sputtering

RF saçtırma ile üretilen SnS ince filmlerine $SnCl_2$ ısıl işleminin etkisi

Ali Çiriş[1,*]

[1] *Niğde Ömer Halisdemir University, Nanotechnology Application and Research Center, 51240, Niğde Türkiye*

Abstract

In this study, the effect of $SnCl_2$ treatment on SnS thin films was investigated. SnS thin films were grown by RF sputtering and $SnCl_2$ treatment was applied by wet chemical processing. While the samples grouped as $SnCl_2$ heat treated and annealed were subjected to annealing in air atm, the as-deposited sample was not applied any annealing process. The as-deposited sample grew in the orthorhombic SnS phase. Annealing of the SnS sample in air environment led to the formation of orthorhombic SnS as well as non-dominant SnS_2 and SnO_2 phases. It was found that applying $SnCl_2$ heat treatment to SnS deteriorated the crystallization and especially the SnO_2 oxide phase became more dominant. Raman spectra confirmed the presence of SnS and SnS_2 phases in the samples, but no evidence of SnO_2 phase was found. SEM images showed bladelike, dense grain formation in the as-deposited and annealed samples. However, $SnCl_2$ heat treatment completely changed the surface morphology of the sample, causing it to transform into a structure consisting of several domains split by deep fractures. EDS revealed a distinct Sn-rich composition of the as-deposited and annealed samples (Sn/S~1.2). On the other hand, $SnCl_2$ heat treatment caused a massive loss of sulphur in the atomic distribution of the SnS and it was seen that the Sn/S ratio increased to around 7.5. The band gaps of the as-deposited and annelaed samples were calculated as 1.43 eV and 1.45, respectively. However, $SnCl_2$ heat treatment led to an increase to 1.56 eV of the band gap. Analysis results show that $SnCl_2$ treatment by the wet processing causes a significant change on the characteristics of SnS thin film. In this context, it can be said that $SnCl_2$ heat treatment can be further improved with optimization processes.

Keywords: SnS, $SnCl_2$ treatment, RF sputtering, air annealing

Öz

Bu çalışmada $SnCl_2$ işleminin SnS ince filmlerine etkisi araştırıldı. SnS ince filmleri, RF saçtırma ile büyütülürken, $SnCl_2$ işlemi ıslak kimyasal yöntem ile uygulandı. $SnCl_2$ ısıl işlemi uygulanan ve tavlanan olarak gruplandırılan örnekler, hava atmosferinde ısıl işlemine tabi tutulurken, tavlanmayan örneğe herhangi bir ısıl işlem uygulanmadı. Hiçbir işlem uygulanmayan örnek, ortorombik SnS fazında büyüdü. SnS örneğinin hava ortamında tavlanması, ortorombik SnS'nin yanı sıra baskın olmayan SnS_2 ve SnO_2 fazlarının oluşumuna neden oldu. SnS'ye $SnCl_2$ ısıl işlemi uygulanmasının kristallenmeyi kötüleştirdiği ve özellikle SnO_2 oksit fazının daha baskın hale getirdiği görüldü. Raman spektrumları, numunelerde SnS ve SnS_2 fazlarının varlığını doğruladı, ancak SnO_2 fazına dair bir bulguya rastlanmadı. SEM görüntüleri, işlem uygulanmayan ve tavlanan örneklerde bıçağa benzeyen, yoğun tane oluşumu sergiledi. Bununla birlikte, $SnCl_2$ ısıl işlemi, numunenin yüzey morfolojisini tamamen değiştirerek, derin kırıklarla bölünen birkaç bölgeden oluşan bir yapıya neden oldu. EDS, işlem uygulanmayan ve tavlanan numunelerin belirgin bir Sn zengini kompozisyonunu ortaya çıkardı (Sn/S~1.2). $SnCl_2$ ısıl işlemi ise SnS'nin atomik dağılımında büyük bir kükürt kaybına neden olarak Sn/S oranının 7.5 civarına yükselmesine yol açtı. İşlem görmeyen ve tavlanan örneklerin bant aralıkları, sırasıyla 1.43 eV ve 1,45 olarak hesaplandı. Bununla birlikte, $SnCl_2$ ısıl işlemi, bant aralığının 1.56 eV'ye yükselmesine neden oldu. Analiz sonuçları, ıslak kimyasal yöntem ile $SnCl_2$ ısıl işlemi uygulanmasının SnS ince filmlerin özelliklerinde ciddi bir değişime neden olduğunu göstermektedir. Bu bağlamda, $SnCl_2$ ısıl işleminin optimizasyon süreçleriyle daha da geliştirilebileceği söylenebilir.

Anahtar kelimeler: SnS, $SnCl_2$ işlemi, RF saçtırma, havada tavlama

1 Introduction

SnS semiconductor material has substituted in the photovoltaic world as environmentally friendly, cost-effective materials with features such as suitable band gap, high absorption coefficient, p-type conductivity, and binary structure [1]. In SnS solar cells, a record efficiency of 4.36% has been achieved so far, although the theoretical cell efficiency of about 30% is predicted [2, 3]. In order to improve the device efficiency, it is necessary to develop material properties such as crystallization quality, grain structure, defect structure, and carrier concentration which limit cell efficiency [4]. In this context, researches on deposition with various methods (RF sputtering, spray pyrolysis, thermal evaporation, close space sublimation, etc.) and optimization of deposition parameters have been carried out [5, 6].

One of the most effective ways to improve the characteristics of SnS thin films is post-deposition heat treatment. This is usually accomplished by annealing the materials in various atmospheres after growing SnS thin

* Sorumlu yazar / Corresponding author, e-posta / e-mail: aliciris@ohu.edu.tr (A. Çiriş)
Geliş / Recieved: 22.03.2023 Kabul / Accepted: 23.05.2023 Yayımlanma / Published: 15.07.2023
doi: 10.28948/ngumuh.1269037

films [7, 8]. Besides, one of the most promising applications for post-deposition process may be also chlorination treatment. The mainstay of the chlorination step for SnS thin films is the fact that the device performance is improved by applying the $CdCl_2$ treatment on CdTe absorption layers. It was observed that the application of $CdCl_2$ treatment on CdTe increased the grain size, reduced grain boundaries and defectivity, and improved heterojunction quality [9, 10]. In this sense, $SnCl_2$ can be used for the chlorination of SnS thin films instead of $CdCl_2$ used for CdTe. There is a limited number of studies examining $SnCl_2$ treatment to SnS thin films. Di Mare et al. showed that recrystallization and improvement of grain quality can be provided with $SnCl_2$ treatment at high temperatures in SnS films produced by close space sublimation method [11]. Spalatu et al. coated a thin $SnCl_2$ layer on the SnS films deposited by the close space sublimation and annealed at different temperatures. It was revealed that $SnCl_2$ treatment caused the formation of liquid flux, assisting grain growth by favor of recrystallization [12]. The above explanations infer that $SnCl_2$ treatment has a significant effect on the characteristic properties of SnS thin films. Therefore, the effect of $SnCl_2$ treatment on SnS produced under different conditions should be investigated.

In this study, SnS layers were produced by RF sputtering method due to quality and controlled deposition process. Then $SnCl_2$ treatment was applied using wet chemical processing method. Using a detailed analysis of the structural and optical properties of the samples annealed in air atmosphere, the effect of $SnCl_2$ treatment on SnS thin films was investigated.

2 Material and methods

In order to examine the effect of $SnCl_2$ treatment on the structural and optical properties of SnS thin films, the samples were grown on soda lime glass (SLG) substrates. Before deposition, the glass substrates were carefully cleaned using acetone, isopropanol, and de-ionized water, respectively.

SnS thin films were coated on the substrates by RF sputtering method. Details on the sputtering system are specified in Ref. [8]. The thin films were grown using single SnS target in high purity. The growth of the films was performed at Ar working pressure of 6 mTorr. Also, SnS layers were deposited at a substrate temperature of 300°C to improve the film quality and at a rotational speed of 8 rpm for homogeneous growth of the films. The deposition was performed at 44 W RF power with a growth rate of 0.9 Å/s. The thickness of the SnS films was set to about 1 µm. Then, the deposited films were divided into three groups for comparison the effect of $SnCl_2$ treatment.

i) SnS sample with $SnCl_2$ heat treatment ($SnCl_2$ treated SnS): After growing SnS thin film by RF sputtering, $SnCl_2$ treatment was applied to it by wet chemical processing. Firstly, the $SnCl_2$ solution used in the treatment was obtained by dissolving 0.62 g $SnCl_2.2H_2O$ powder in 5 mL of ethanol. Then, the $SnCl_2$ treatment was carried out by dripping a solution of 1 drop/cm^2 on the film surface, followed by drying the sample at 60°C. Finally, the SnS/$SnCl_2$ structure was post-annealed at 300°C for 15 min in air atmosphere using the conventional tube furnace.

ii) SnS annealed without $SnCl_2$ (annealed SnS): After SnS thin film was deposited by RF sputtering, it was post-annealed at 300°C in air atmosphere for 15 minutes using a conventional tube furnace.

iii) As-deposited SnS: no process was applied after growing SnS thin film.

In this context, all samples used in the study are shown schematically in Figure 1.

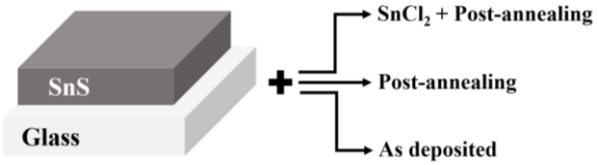

Figure 1. Schematic representation of SnS samples used in the study

The crystallization properties and structural parameters of the samples were examined with X-ray diffractometer (XRD) using CuK_α radiation (λ = 1.5406 Å). Raman spectra as a complementary structural analysis were measured with confocal Raman microscope at a wavelength of 633 nm. Morphological features were examined with the scanning electron microscope (SEM) instrument. Atomic ratios were determined with energy dispersive X-ray spectroscopy (EDS). Optical properties were analyzed with the spectroscopic ellipsometer.

3 Results and discussions

3.1 XRD spectra

In order to investigate the crystallographic effect of $SnCl_2$ heat treatment on SnS films, the XRD spectra of the samples are shown in Figure 2. The XRD spectrum of the as-deposited SnS sample, which did not undergo any heat treatment, showed the SnS phase structure crystallized in the orthorhombic structure (Card No: 00-039-0354). Annealing of the SnS at 300°C for 15 min led to recrystallization. In the sample, the orthorhombic structure of SnS slightly improved and a rather weak hexagonal SnS_2 phase emerged (Card No: 00-023-0677). In addition, the tetragonal SnO_2 phase was formed with the effect of annealing in air atmosphere (Card No: 00-001-0625). It can be said that this phase is taken place as a result of the reaction of Sn atoms in SnS thin films with oxygen molecules in air. In this context, it has also been shown that SnO_2 phase can be formed by annealing in air under suitable conditions [13].

Processing the SnS thin film with the $SnCl_2$ treatment markedly deteriorated the crystallization of the sample. Therefore, deconvolution operation was applied to make the diffraction peaks clearer. According to the deconvolution results, heat treatment with $SnCl_2$ did not change the orthorhombic phase structure of SnS. However, it led to the SnS_2 secondary phase and more strong formation of SnO_2 phase, compared to the annealed SnS sample.

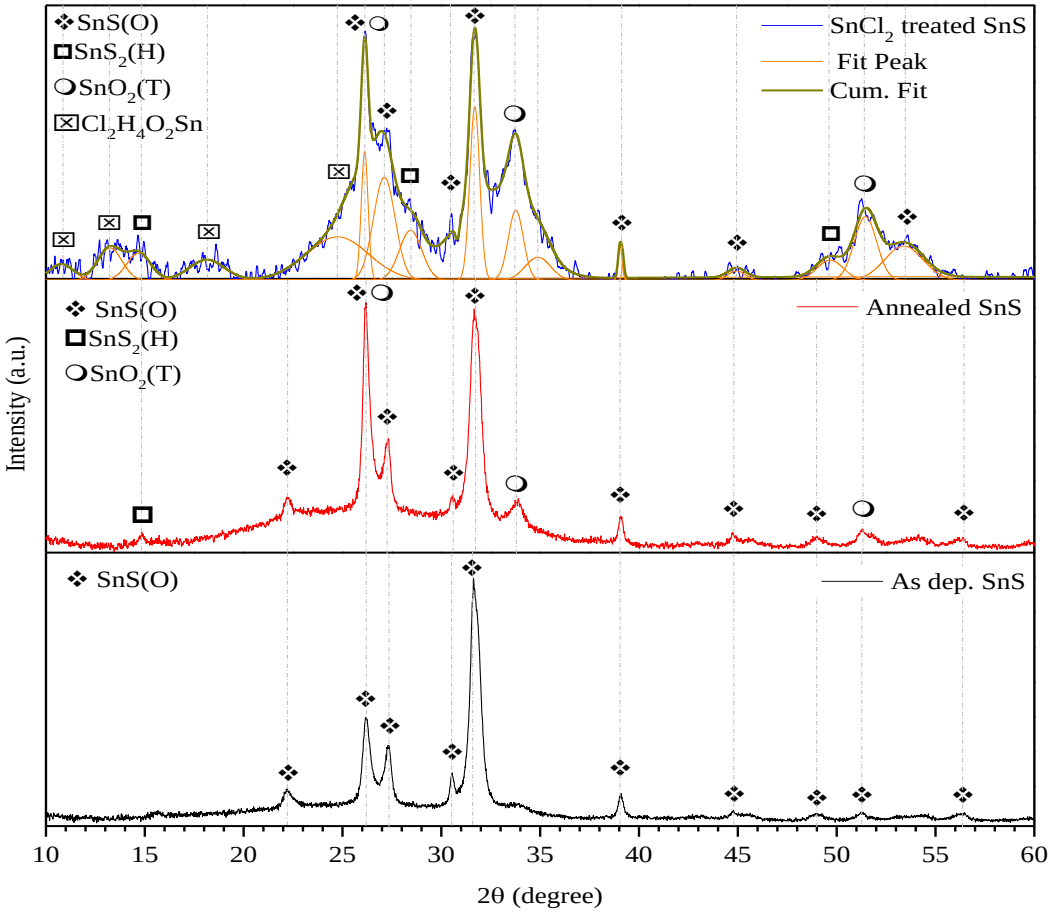

Figure 2. XRD patterns of SnS samples used in the study

In addition, the presence of some recessive peaks belonging to the $Cl_2H_4O_2Sn$ compound used for the chlorination solution was also revealed (Card No: 00-001-0521). The reason for the formation of the $Cl_2H_4O_2Sn$ phase may be due to the residual chlorination solution. On the other hand, this may have remained on the film structure due to not using dilute solution for chlorination and not rinsing the sample after final annealing.

The XRD results of the samples revealed that annealing of SnS in air atmosphere promoted the formation of strange phases. On the other hand, the $SnCl_2$ treatment prepared the infrastructure for the undesirable phases to become more evident.

In order to specify the structural parameters of the samples, the values of crystallite size (D), micro-strain (ε), and dislocation density (δ) were calculated using Equation (1-3) [14].

$$D = \frac{K\lambda}{\beta_{hkl}\cos\theta} \quad (1)$$

$$\varepsilon = \frac{\beta_{hkl}\cos\theta}{4} \quad (2)$$

$$\delta = \frac{1}{D^2} \quad (3)$$

this equations, the symbols K , λ , β_{hkl} and θ denote the Scherrer constant (K=0.94), the X-ray wavelength (λ=1.5406 Å), the full width at half maximum (FWHM) and the Bragg's angle, respectively. The calculations were performed according to (111) orientation of the orthorhombic SnS phase. The calculation results for the structural parameters are presented in Table 1. As seen in Table, the crystallite size for the as-deposited sample was determined as 15.6 nm. The crystal size was slightly reduced in the annealed sample, while it decreased down to 12.7 nm in the $SnCl_2$ treated sample. On the other hand, the strain values and dislocation densities increased in the annealed and $SnCl_2$ treated samples compared to the as-deposited sample. All these values show that orthorhombic SnS deteriorates the crystallization in annealed and $SnCl_2$ heat treated samples.

Table 1. The structural parameters of the samples

Sample	D (nm)	ε (x10^{-3})	δ (x10^{15})
As-deposited	15.6	2.3	4.1
Annealed	14.1	2.6	5.0
$SnCl_2$ treated	12.7	2.9	6.2

3.2 Raman spectra

The Raman spectra of the SnS samples are shown in Figure 3. In the figure, there are Raman modes at 163, 188, 224, 264, and 290 cm^{-1} in the as-deposited SnS sample without any heat treatment. While the bands at 188, 224 and 264 cm^{-1} of these peaks belong to A_g mode of the SnS structure; the bands at 163 and 290 cm^{-1} are attributed to the B_{2g} mode of the SnS [15-17].

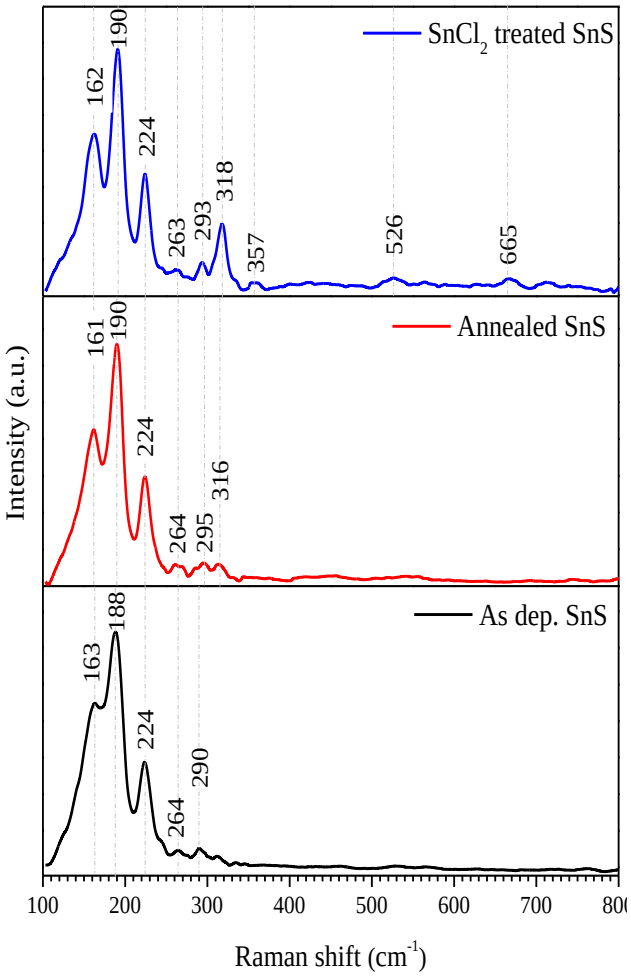

Figure 3. Raman spectra of SnS samples

Annealing of the SnS sample resulted in Raman peaks similar to the as-deposited sample, revealing the presence of SnS phase. In addition, it can be said that the crystallization of the SnS phase is higher than that of the as-deposited sample with the effect of annealing in air atmosphere. Besides, it was noted that the peak of the B_{2g} mode at 161 cm^{-1} was revealed more sharply [18]. In addition, a weak peak recorded at 316 cm^{-1} is attributed to the A_{1g} mode of the SnS_2 phase [19, 20]. In the heat treated SnS thin film with $SnCl_2$, the well-crystallized SnS phase was exposed. Besides, the A_{1g} mode of SnS_2, which appeared weakly in the annealed sample, appeared more dominantly with a slight shift, due to the re-crystallization process resulting from the effect of $SnCl_2$ heat treatment. Unlike the annealed sample, Raman modes appeared at 357, 526, and 665 cm^{-1}, which are attributed to the SnO_2 surface phonon modes in the $SnCl_2$ treated sample [21].

The results of Raman spectra are considerably compatible with XRD data. The minor differences are due to the nature of the Raman analysis technique, collecting data from regions close to the surface rather than deep regions. Thus, it only gives information about the phase structures up to a certain depth of the surface. Since XRD scans the film through its depth, it collects data from a wider region and the presence of different phase structures can also be detected.

3.3 SEM Images

Surface photographs of the samples are shown in Figure 4. The as-deposited SnS sample shown in Figure 4a has rough grain morphology randomly distributed over the substrate with a dense, bladelike grain structure [22]. Annealing of SnS in air atm (Figure 4b) did not cause a significant change in the morphological structure. However, annealing the SnS thin film after $SnCl_2$ treatment led to a radical change in the surface morphology, as can be seen in Figure 4c. The $SnCl_2$ treatment resulted in the surface structure being composed of several domains split by deep fractures. The reason for this interesting surface structure may be its atomic ratios and/or the presence of the strong oxide phase [11].

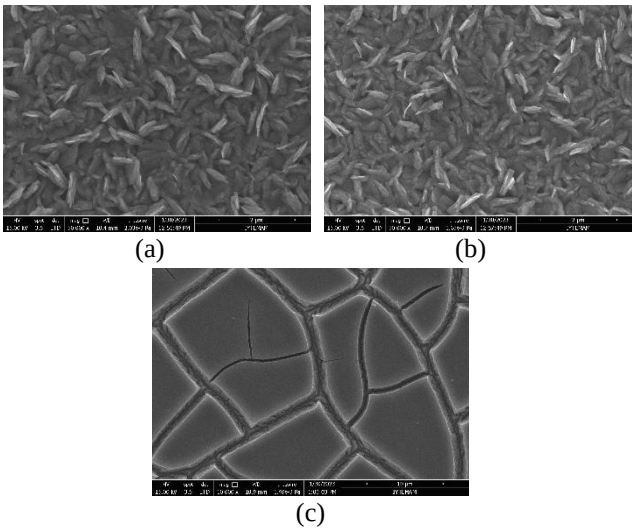

Figure 4. SEM images of the samples of a) as-deposited, b) annealed, c) $SnCl_2$ treated

3.4 EDS Results

The EDS spectra of the samples produced to examine the effect of $SnCl_2$ heat treatment on SnS films are shown in Figure 5. The atomic ratios of the samples obtained using the EDS spectra are presented in Table 2. In the table, it was revealed that SnS without any treatment was grown as Sn-rich (Sn/S ~1.17) and thus, sulfur loss occurred in the growth process of the films. This may be due to the fact that the 'Sn' atoms with higher atomic mass have lower mobility than 'S' atoms at the substrate temperature of 300°C used to grow the films, and therefore the loss of S atoms is greater compared

to Sn [23]. Annealing of SnS in air atmosphere led to a slight increase in the proportion of Sn (Sn/S~1.21).

The application of $SnCl_2$ heat treatment to the SnS film caused a significant change in the atomic ratios. $SnCl_2$ treatment gave rise to a significant loss of sulfur, resulting in a Sn/S ratio of about 7.48. This may be due to the inclusion of extra Sn atom in the SnS structure due to the presence of Sn atoms in the $SnCl_2$ solution, resulting in an increment in the Sn/S ratio. In addition, a significant amount of Cl was released due to the $SnCl_2$ heat treatment. This is because the samples were not rinsed after the heat treatment step and the applied experimental conditions were not sufficient to remove the chlorine from the structure. This is also evident in the XRD spectra.

Table 2. Atomic ratios of the SnS samples

Sample	Sn (%)	S (%)	Cl (%)
As-deposited	54.01	45.99	-
Annealed	54.68	45.32	-
$SnCl_2$ treated	80.01	10.70	9.29

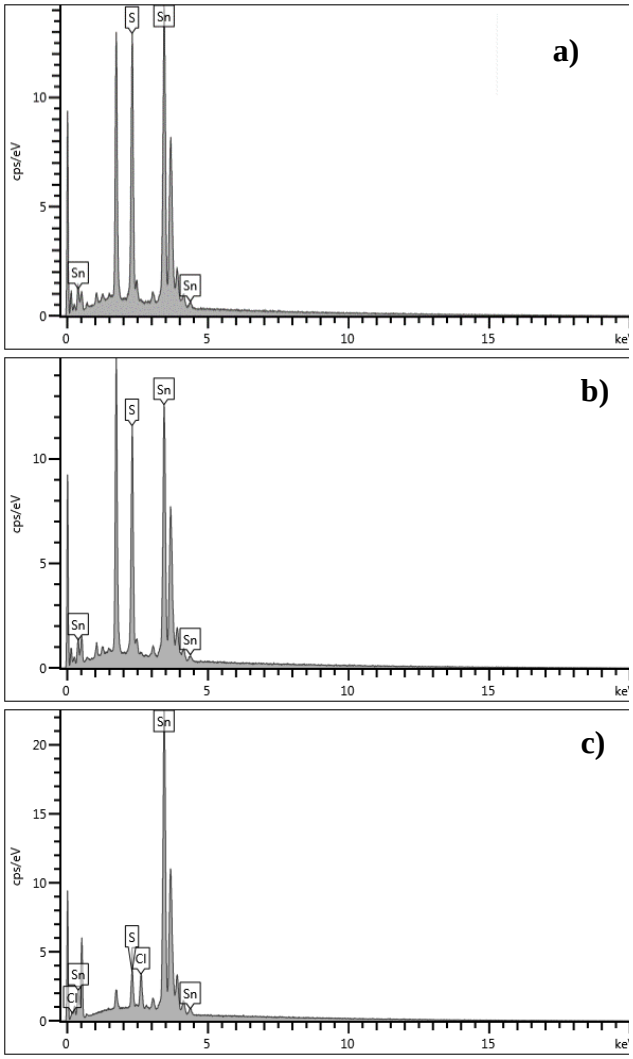

Figure 5. EDS spectra of the samples a) as-deposited, b) annealed, and c) $SnCl_2$ treated

3.5 *Optical properties*

In order to survey the optical properties of the samples, the measurements of optical absorbance versus wavelength were performed in the range of 400-1300 nm. Using the absorbance measurements, the absorption coefficients (α) were calculated using Equation (4).

$$\alpha = 2.303\frac{A}{d} \quad (4)$$

where 'A' is absorbance and d is the thickness of the material. Figure 6 shows the variation of the absorption coefficient with wavelength. The absorbance graph of the samples is also presented in the inset of the figure. The absorbance curves show that the absorption edges of the samples are in the near-infrared region and annealing of the as-deposited SnS with/without $SnCl_2$ causes a slight shift to the short wavelength region. In addition, all SnS samples exhibited a high optical absorption coefficient (~10^5 cm^{-1}) in the visible region.

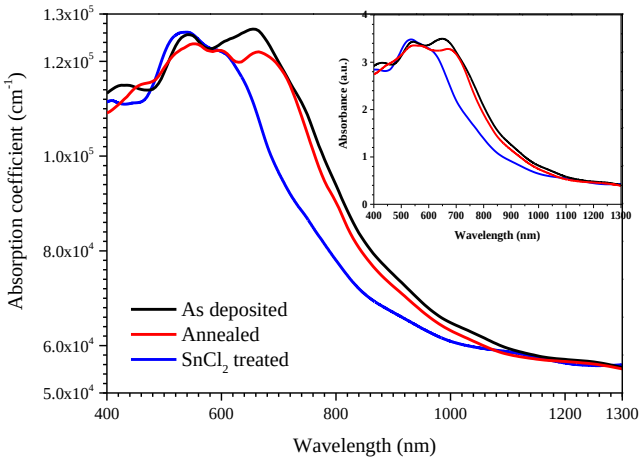

Figure 6. The variation graph of absorption coefficients versus wavelength of the samples (Inset: absorbance curves of the samples)

The band gap of thin film material can be calculated by Tauc method using Equation (5) [24].

$$(\alpha h\nu) = C(h\nu - E_g)^n \quad (5)$$

In this equation, E_g is the band gap, C is the proportionality constant, $h\nu$ is the photon energy 'α' is the absorption coefficient, and 'n' is a value depending on the nature of the transition. The 'n' value is equal to 1/2 for direct-transition materials and 2 for indirect-transition. However, 'n' was taken as 1/2, due direct-transitive nature of the SnS films used in our study. In this context, the $(\alpha h\nu)^2$-$h\nu$ graph drawn to determine the band gap is shown in Figure 7. In the figure, band gap values are calculated with the point in which the linear part of the curve intersects the x-axis [25]. The calculated band gap values of the sample are presented in Table 3. As seen in Table, the band gap of the as-deposited SnS sample without any heat treatment was calculated as about 1.43 eV. On the other hand, annealing of the SnS film

caused the band gap to increase slightly (~1.45 eV). The application of $SnCl_2$ heat treatment to the SnS led to the band gap changing significantly, increasing to 1.56 eV.

The band gap values of as-deposited and annealed SnS samples are in agreement with previous studies [8, 26]. However, it can be said that the variation in the band gap of the $SnCl_2$ treated sample is related to the surface morphology and composition [27].

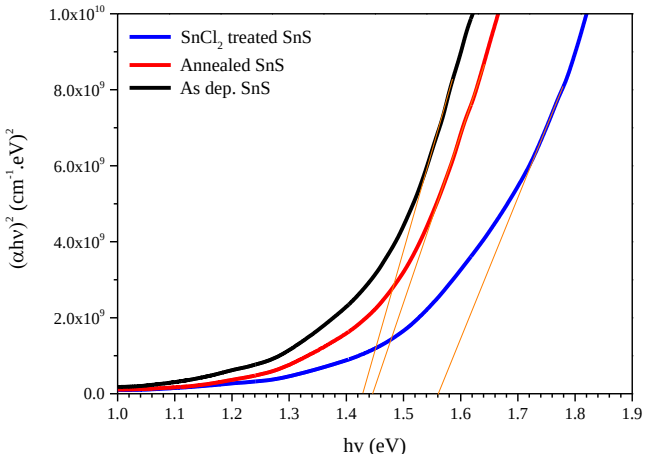

Figure 7. $(\alpha h\nu)^2$-hν graphs of the samples

Urbach energy (E_U) associates the localized states with lattice disorder and crystal defects [28]. E_U values of the samples can be determined using Equation (6) [29].

$$\alpha = \alpha_o \exp\left[\frac{h\nu}{E_U}\right] \quad (6)$$

where 'α' is the absorption coefficient, 'α_o' is constant, 'E_g' is the band gap, and 'E_U' is Urbach energy. In the In(α)-hν curve obtained by deriving from this formula, the inverse of the slope gives the Urbach energy value. The obtained Urbach energy values are shown in Table 3. The table shows that annealing of the as-deposited sample caused a slight increase in Urbach energy. However, $SnCl_2$ treatment led to a significant increase, due to an increment in disorder and deterioration in crystallinity [28, 30].

Table 3. Urbach energies and band gap values of the samples

Sample	Urbach energy (eV)	Bang gap (eV)
As-deposited	0.68	1.43
Annealed	0.69	1.45
$SnCl_2$ treated	0.95	1.56

4 Conclusions

In this study, the impact of $SnCl_2$ heat treatment on the structural and optical properties of SnS thin films deposited by RF sputtering was examined. While it was determined that the as-deposited sample without any treatment crystallized in the orthorhombic SnS phase, annealing of SnS at 300°C for 15 minutes in air atmosphere led to the formation of non-dominant SnS_2 secondary phase and SnO_2 structure together with orthorhombic SnS as a result of recrystallization. Heat treatment of SnS with $SnCl_2$ resulted in a significant deterioration of crystallization. The deconvolution process applied to determine the phase structure showed the orthorhombic SnS phase, the intensified SnS_2 and SnO_2 phases as well as $Cl_2H_4O_2Sn$ compound due to the residual chlorination solution. The orthorhombic SnS phase was seen in all samples in Raman spectra. Besides, SnS_2 phase was revealed in the annealed and $SnCl_2$ heat treated samples. The SnO_2 phase that appeared in the XRD spectrum was only seen in the Raman spectrum of the $SnCl_2$ treated SnS sample. SEM images showed the bladelike, dense, and coarse-grained structure of the as-deposited and the annealed samples. However, it turned out that the $SnCl_2$ treated sample had a morphology consisting of several domains. In EDS analysis, it was determined that as-deposited and the annealed samples were Sn-rich (Sn/S~1.2), however, $SnCl_2$ treatment severely affected the atomic composition, resulting in Sn/S ratio of about 7.5. In optical calculations, the band gaps of as-deposited SnS and annealed SnS were detected as 1.43 eV and 1.45 eV, respectively. The band gap of $SnCl_2$ treated SnS was calculated to be 1.56 eV with a significant increment. It can be said that this increase is due to the obvious changes in the grain structure and composition of the sample. In addition, the Urbach energy associated with the structural disorders was calculated as 0.68 eV for the as-deposited sample, while the annealed sample did not significantly change. However, the $SnCl_2$ process caused a significant increase.

Acknowledgment

A. Çiriş would like to thank to Y. Atasoy for the XRD, SEM and EDS measurements and M.A. Olgar for the material source.

Conflict of interest

The author declares that there is no conflict of interest.

Similarity rate (iThenticate): 15%

References

[1] K.R. Reddy, N.K. Reddy, R. Miles, Photovoltaic properties of SnS based solar cells. Solar energy materials and solar cells, 90 (18-19), 3041-3046, 2006, https://doi.org/10.1016/j.solmat.2006.06.012.

[2] P. Sinsermsuksakul, L. Sun, S.W. Lee, H.H. Park, S.B. Kim, C. Yang, R.G. Gordon, Overcoming efficiency limitations of SnS-based solar cells. Advanced Energy Materials, 4 (15), 1400496, 2014, https://doi.org/10.1002/aenm.201400496.

[3] W. Shockley, H.J. Queisser, Detailed balance limit of efficiency of p-n junction solar cells. Journal of Applied Physics, 32 (3), 510-519, 1961, https://doi.org/10.1063/1.1736034.

[4] S. Di Mare, D. Menossi, A. Salavei, E. Artegiani, F. Piccinelli, A. Kumar, G. Mariotto, A. Romeo, SnS thin film solar cells: perspectives and limitations. Coatings, 7 (2), 34, 2017, https://doi.org/10.3390/coatings7020034.

[5] N. Koteeswara Reddy, M. Devika, E. Gopal, Review on tin (II) sulfide (SnS) material: synthesis, properties,

and applications. Critical Reviews in Solid State and Materials Sciences, 40 (6), 359-398, 2015, https://doi.org/10.1080/10408436.2015.1053601.

[6] R. Banai, M. Horn, J. Brownson, A review of tin (II) monosulfide and its potential as a photovoltaic absorber. Solar energy materials and solar cells, 150, 112-129, 2016, https://doi.org/10.1016/j.solmat.2015.12.001.

[7] N. Revathi, S. Bereznev, M. Loorits, J. Raudoja, J. Lehner, J. Gurevits, R. Traksmaa, V. Mikli, E. Mellikov, O. Volobujeva, Annealing effect for SnS thin films prepared by high-vacuum evaporation. Journal of Vacuum Science & Technology A: Vacuum, Surfaces, and Films, 32 (6), 061506, 2014, https://doi.org/10.1116/1.4896334.

[8] M. Olgar, A. Çiriş, M. Tomakin, R. Zan, Impact of in/ex situ annealing and reaction temperature on structural, optical and electrical properties of SnS thin films. Journal of Molecular Structure, 1241, 130631, 2021, https://doi.org/10.1016/j.molstruc.2021.130631.

[9] I.M. Dharmadasa, Review of the $CdCl_2$ Treatment Used in CdS/CdTe Thin Film Solar Cell Development and New Evidence towards Improved Understanding. Coatings, 4 (2), 282-307, 2014, http://doi.org/10.3390/coatings4020282.

[10] N.A. Shah, Z. Rabeel, M. Abbas, W.A. Syed, Effects of CdCl2 treatment on physical properties of CdTe/CdS thin film solar cell. Modern Technologies for Creating the Thin-film Systems and Coatings, 2017, http://dx.doi.org/10.5772/67191.

[11] S. Di Mare, A. Salavei, D. Menossi, F. Piccinelli, P. Bernardi, E. Artegiani, A. Kumar, G. Mariotto, A. Romeo, A study of SnS recrystallization by post deposition treatment. 2016 IEEE 43rd Photovoltaic Specialists Conference (PVSC), 0431-0434, 2016, http://doi.org/10.1109/PVSC.2016.7749627.

[12] N. Spalatu, J. Hiie, R. Kaupmees, O. Volobujeva, J. Krustok, I. Oja Acik, M. Krunks, Postdeposition processing of SnS thin films and solar cells: prospective strategy to obtain large, sintered, and doped SnS grains by recrystallization in the presence of a metal halide flux. ACS Applied Materials & Interfaces, 11 (19), 17539-17554, 2019, https://doi.org/10.1021/acsami.9b03213.

[13] S.C. Ray, M.K. Karanjai, D. DasGupta, Structure and photoconductive properties of dip-deposited SnS and SnS2 thin films and their conversion to tin dioxide by annealing in air. Thin Solid Films, 350 (1-2), 72-78, 1999, https://doi.org/10.1016/S0040-6090(99)00276-X.

[14] B.H. Baby, D.B. Mohan, The effect of in-situ and post deposition annealing towards the structural optimization studies of RF sputtered SnS and Sn2S3 thin films for solar cell application. Solar Energy, 189, 207-218, 2019, https://doi.org/10.1016/j.solener.2019.07.059.

[15] V.R.M. Reddy, S. Gedi, C. Park, R. Miles, R.R. KT, Development of sulphurized SnS thin film solar cells. Current Applied Physics, 15 (5), 588-598, 2015, https://doi.org/10.1016/j.cap.2015.01.022.

[16] H. Chandrasekhar, R. Humphreys, U. Zwick, M. Cardona, Infrared and Raman spectra of the IV-VI compounds SnS and SnSe. Physical Review B, 15 (4), 2177, 1977, https://doi.org/10.1103/PhysRevB.15.2177.

[17] S. Sohila, M. Rajalakshmi, C. Ghosh, A. Arora, C. Muthamizhchelvan, Optical and Raman scattering studies on SnS nanoparticles. Journal of Alloys and Compounds, 509 (19), 5843-5847, 2011, https://doi.org/10.1016/j.jallcom.2011.02.141.

[18] J.M. Skelton, L.A. Burton, A.J. Jackson, F. Oba, S.C. Parker, A. Walsh, Lattice dynamics of the tin sulphides SnS_2, SnS and Sn_2S_3: vibrational spectra and thermal transport. Physical Chemistry Chemical Physics, 19 (19), 12452-12465, 2017, https://doi.org/10.1039/C7CP01680H.

[19] A. Smith, P. Meek, W. Liang, Raman scattering studies of SnS2 and SnSe2. Journal of Physics C: Solid State Physics, 10 (8), 1321, 1977, https://doi.org/10.1088/0022-3719/10/8/035.

[20] N. Revathi, S. Bereznev, J. Iljina, M. Safonova, E. Mellikov, O. Volobujeva, PVD grown SnS thin films onto different substrate surfaces. Journal of Materials Science: Materials in Electronics, 24, 4739-4744, 2013, http://doi.org/10.1007/s10854-013-1468-8.

[21] R. Mariammal, K. Ramachandran, B. Renganathan, D. Sastikumar, On the enhancement of ethanol sensing by CuO modified SnO2 nanoparticles using fiber-optic sensor. Sensors and Actuators B: Chemical, 169, 199-207, 2012, https://doi.org/10.1016/j.snb.2012.04.067.

[22] O.V. Bilousov, Y. Ren, T. Törndahl, O. Donzel-Gargand, T. Ericson, C. Platzer-Björkman, M. Edoff, C. Hägglund, Atomic layer deposition of cubic and orthorhombic phase tin monosulfide. Chemistry of Materials, 29 (7), 2969-2978, 2017, https://doi.org/10.1021/acs.chemmater.6b05323.

[23] V.K. Arepalli, Y. Shin, J. Kim, Influence of working pressure on the structural, optical, and electrical properties of RF-sputtered SnS thin films. Superlattices and Microstructures, 122, 253-261, 2018, https://doi.org/10.1016/j.spmi.2018.08.001.

[24] J. Tauc, R. Grigorovici, A. Vancu, Optical properties and electronic structure of amorphous germanium. physica status solidi (b), 15 (2), 627-637, 1966, http://doi.org/10.1002/pssb.19660150224.

[25] P. Makuła, M. Pacia, W. Macyk, How to correctly determine the band gap energy of modified semiconductor photocatalysts based on UV–Vis spectra. 9 (23), 6814-6817, 2018, https://doi.org/10.1021/acs.jpclett.8b02892.

[26] J. Xu, Y. Yang, Z. Xie, Effect of vacuum annealing on the properties of sputtered SnS thin films. Chalcogenide Letters, 11 (10), 485-491, 2014.

[27] P. Jain, P. Arun, Influence of grain size on the band-gap of annealed SnS thin films. Thin Solid Films, 548, 241-246, 2013, https://doi.org/10.1016/j.tsf.2013.09.089.

[28] P. Norouzzadeh, K. Mabhouti, M. Golzan, R. Naderali, Investigation of structural, morphological and optical characteristics of Mn substituted Al-doped ZnO NPs: a Urbach energy and Kramers-Kronig study. Optik, 204, 164227, 2020, https://doi.org/10.1016/j.ijleo.2020.164227.

[29] F. Urbach, The long-wavelength edge of photographic sensitivity and of the electronic absorption of solids. Physical review, 92 (5), 1324, 1953.

[30] M. Messaoudi, S. Boudour, Extent of dependence of crystalline, morphological, optical and electrical properties on deposition time of sprayed SnS thin films. Microscopy Research and Technique, 86 (3), 342-350, 2023, https://doi.org/10.1002/jemt.24275.